

## TWO SCALE PORE ANALYSIS APPLIED TO LOW PERMEABILITY SANDSTONE

C. A. Davy<sup>1</sup>, P.M. Adler<sup>2</sup>, Yang Song<sup>1</sup>, L. Jeannin<sup>3</sup>, D. Troadec<sup>4</sup>, G. Hauss<sup>1</sup>, Thang Nguyen Kim<sup>2</sup>

<sup>1</sup> LML UMR CNRS 8107/Ecole Centrale de Lille, CS20048,  
59651 Villeneuve d'Ascq Cedex, France

<sup>2</sup> Metis/UPMC, Paris, France

<sup>3</sup> GDFSUEZ E&P International SA, 1 place Samuel de Champlain,  
92930 Paris La Défense cedex - France

<sup>4</sup> IEMN, UMR CNRS 8520, BP60069, 59652 Villeneuve d'Ascq Cedex, France

*This paper was prepared for presentation at the International Symposium of the Society of Core Analysts held in St. John's Newfoundland and Labrador, Canada, 16-21 August, 2015*

### ABSTRACT

The purpose of this research is 1) to predict fluid transport (permeability) from pore structure measurements of a tight gas sandstone and 2) to compare predictions to actual permeability measurements on centimetric plugs. This contributes to explain what is (or are) the relevant pore scale(s) for fluid transport, and should help improve gas production. Tight sandstones are low porosity media, with small fluid transport ability. The sample T-2390-82 used in this contribution has a water porosity of 2.8-3.2%, and a dry gas permeability of the order of  $10^{-17} \text{ m}^2$  (10 microDarcy).

The pore size distribution of T-2390-82 is measured by Mercury Intrusion Porosimetry (M.I.P.) with a peak at 350 nm. This justifies the use of Focused Ion Beam/Scanning Electron Microscope (FIB/SEM) to describe the 3D pore structure. FIB/SEM provides the 3D geometry of a single joint (between quartz grains). However, 2D SEM shows the presence of numerous joints of both sub-micrometric and micrometric sizes; 2D SEM is used to describe the joint network topology (density, joint length, etc.). X-ray microtomography (micro-CT) is used in an attempt to describe a representative pore network in 3D. If  $a$  denotes the voxel size, no connected pore network is measured with  $a = 13$  micron, and it is hardly connected with  $a = 4.4$  micron. A voxel size of 600 nm is necessary to image micrometric joints, yet only individual ones.

In order to predict fluid transport, 2D SEM is used to describe the joint network topology and macroscopic permeability, combined to either (1): micro-CT or (2): FIB/SEM for the individual joint transmissivity. At the joint network scale and at the 3D joint scale, two-scale numerical modelling shows that micrometric joints (observed with micro-CT) control macroscopic permeability, although they have a partial volume contribution to porosity, according to MIP. However, sub-micrometric joints (imaged by FIB/SEM) which contribute significantly to porosity (up to 1.27%) are slow paths for fluid transport

(with permeabilities smaller by two to three orders of magnitude, when compared to that given by micrometric joints).

## INTRODUCTION

Low permeability materials are often composed of several pore structures of various scales, which are superposed one to another. It is often impossible to measure and to determine the pore geometry properties relevant for fluid transport in one step, or with a unique experimental device.

In low permeability sandstones, the pore space is essentially made of micro-cracks between grains. These macro-cracks (or fissures) are two dimensional structures, which aperture is roughly on the order of one micron. When considering the grain scale, i.e., on the millimetric scale, fissures form a network.

These two structures (individual crack and fissure network) are measured by using different tools [1]. The density of the fissure network is estimated by trace measurements on the two dimensional images provided by classical 2D Scanning Electron Microscopy (SEM) with a pixel size of about 2 micron. The three dimensional geometry of fissures is measured by both (1) Focused Ion Beam/Scanning Electron Microscopy (FIB/SEM) with voxel size  $a = 15$  nm and (2) X-Ray micro-tomography (micro-CT) in the laboratory ([www. http://isis4d.univ-lille1.fr](http://isis4d.univ-lille1.fr)), with  $a = 0.6$  micron, or 4.37 micron or 13 micron.

A two-step methodology is proposed to predict the transport properties of tight sandstones. It is applied on the example of tight sandstone T-2390-82. Transport is characterised on two different scales; the pore network, representative of the macroscopic scale, is imaged by 2D SEM in terms of crack organisation, average length, density, etc.; the aperture  $b$  of the individual cracks is characterized on the scale given by FIB/SEM for sub-micrometric joints, and by micro-CT for micrometric joints. Numerical calculations are performed first, for the whole pore network (given by 2D SEM), as a function of network characteristics; they yield a permeability proportional to the fracture transmissivity. This individual crack transmissivity is determined by using the geometry of the individual cracks (given by FIB/SEM and micro-CT).

## EXPERIMENTAL

Experiments were performed on a single sample (37.7 mm diameter and 34.6 mm height) of tight sandstone reference T-2390-82, after oven-drying at 105°C until mass stabilization (dry state).

**Macroscopic Dry Gas Permeability.** Details of the experimental method are given in [3]. The 37.7 mm diameter sample is subjected to a quasi-static argon gas flow, at an upstream gas injection pressure of 2 to 4 MPa. The apparent gas permeability  $K_{\text{gas}}$  is measured during a small decrease in upstream gas pressure by 0.05 MPa, during two successive cycles of external hydrostatic stress loading up to 45 MPa. For such important gas injection pressures, the Klinkenberg effect is generally negligible [4]. After these

cycles, the sample is over-cored transversely to a sample of 20mm diameter and 30.8 mm height, and tested for gas permeability again.

Fig. 1 shows that gas permeability  $K_{gas}$  decreases significantly with increasing hydrostatic stress  $P_c$ ; this is attributed to the progressive closure of fissures under loading. For further permeability predictions, an average  $K_{gas}$  of  $2.1 \pm 0.4 \cdot 10^{-17} \text{ m}^2$  (21  $\pm$  4 micro Darcy) is considered at low  $P_c = 2.5$  to 5MPa.

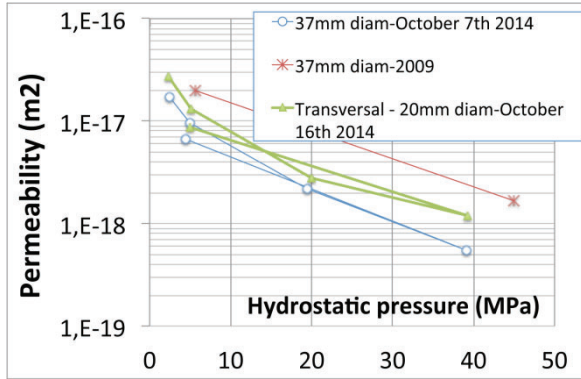


Figure 1: Gas permeability for 37.7mm diameter and perpendicular 20mm diameter T-2390-82 sandstone sample

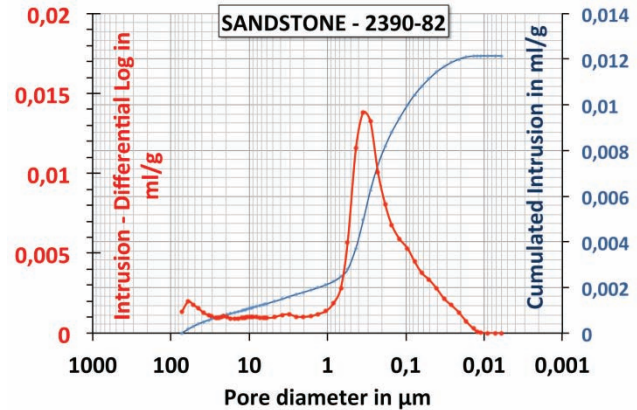


Figure 2: MIP results for T-2390-82 sandstone, plotted after blank cell and conformance corrections [5,6]

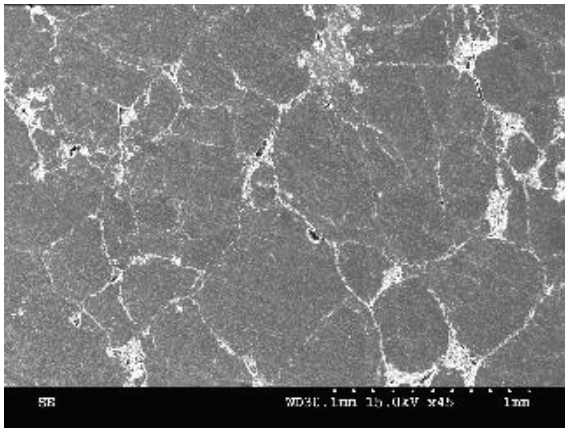


Figure 3: Original 2D SEM image of sample T-2390-82.

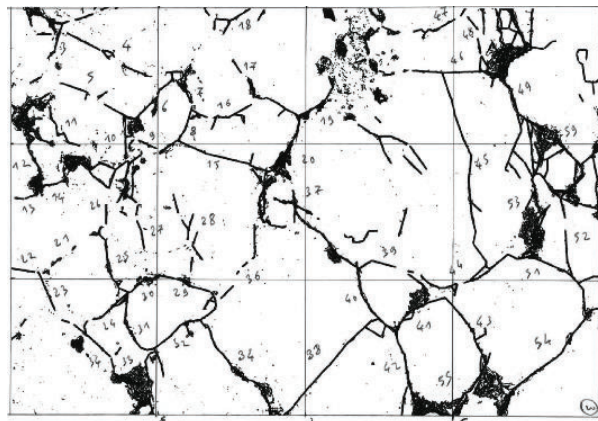


Figure 4: Corresponding trace map of the SEM image (left) used for permeability prediction

**Indirect Pore Structure Assessment.** Porosity  $\phi$  is measured by the water imbibition method on the 37.7 mm sample and on its 20 mm over-cored part; values of 2.8-3.2% are obtained.

Mercury Intrusion Porosimetry is performed using a MICROMERITICS AutoPore IV 9500 up to 200 MPa, which corresponds to intruded pores down to 4 nm. Results (Fig. 2) show a characteristic pore size of about 350 nm, with a limited contribution of pores

between 1-10 microns to cumulative pore size distribution. This justifies the use of FIB/SEM imaging to describe sub-micrometric pores in 3D.

**Direct Characterization of the Pore Structure: 2D SEM.** The pore network cannot be characterized by FIB/SEM alone. 2D SEM measures directly the topology (average length, density, connectivity) of the fissure network of T-2390-82 sandstone. SEM images are taken at low magnification (x40-45), with a pixel size of 2.15-2.33 micron, on the top surface of the 37.7 mm diameter sample, where several zones of different fissure densities are observed. A high fissure density zone and a medium density zone are computed in the following. Therefore, a trace map of each individual SEM image is made by manually locating each individual fissure (Figs. 3 and 4).

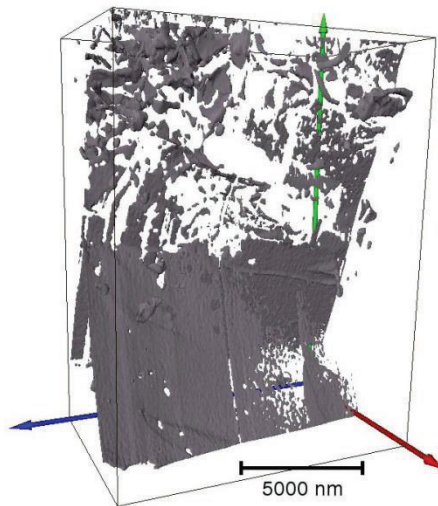


Figure 5: Pore network given by FIB/SEM (3D reconstruction with Amira software, FEI)

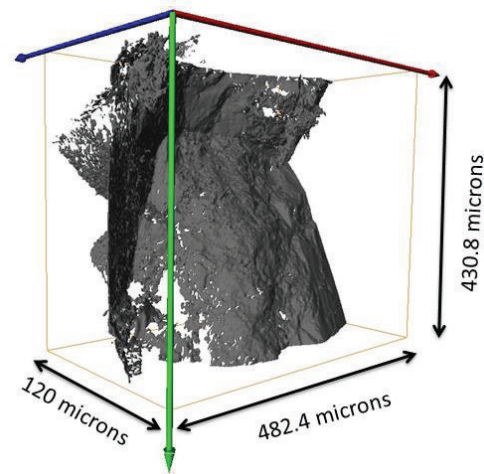


Figure 6: Pore network given by micro-CT on a 0.8mm rod (3D reconstruction with Amira software, FEI)

**Direct Characterization of the Pore Structure: FIB/SEM.** The focused ion beam (FIB) cuts a U-shaped hole in order to isolate a plane-parallel sandstone volume [7]. Following this, the FIB cuts regularly-spaced 50nm thick slices from the plane-parallel volume, perpendicularly to the sample polished surface. Between each FIB cutting, the sandstone matter perpendicular to the polished surface is observed with an electron detector of the in lens type. A stack of 300 images is computed. Sample T-2390-82 has a voxel size of  $14.65 \times 35.71 \times 50.0 \text{ nm}^3$ , and a total investigated volume of  $(9874 \times 20069 \times 15000) \text{ nm}^3$ . The 3D pore network is obtained from the raw FIB/SEM image stack, by filtering and segmentation of each individual image using the ImageJ software. The 3D object is generated by using the Amira (FEI) software, by using the method described in [8] (Fig. 5). The 2D and 3D Continuous Pore Size Distributions (CPSD) are deduced from the binary images, as described by [9].

**Direct Characterization of the Pore Structure: micro-CT.** For comparison purposes, three image series of the same T-2390-82 sample are acquired with three voxel sizes of 13 microns (measured on the 20 mm diameter sample used for gas permeability), 4.4

microns (on a parallelepipedic sample of 5 mm width) and 0.6 microns (on a thin rod of 0.8mm width). Image filtering and segmentation by Image J and 3D visualization by Amira (Fig. 6) are performed as for FIB/SEM.

**Comparison between the Various Pore Structure Assessment Methods.** Indirect and direct methods for pore structure assessment are compared in Table 1. For a = 13 micron and 4.4 micron, pore volumes of micro-CT samples are not connected from one surface to another, despite porosities of 1.016% +/-0.36 and 1.88% +/-0.17. Compared to water porosity (2.8-3.2%), M.I.P. provides a greater value, possibly due to sample damage. On the opposite, micro-CT of the 0.8mm rod provides a connected pore volume (Fig. 6), corresponding to an individual fissure between two quartz grains, of porosity 1.34% +/- 0.15 and average opening of 4 micron. Although significantly smaller, the FIB/SEM sample provides a porosity of 1.25%, which is similar to micro-CT, and a typical opening on the order of 60-100nm. At this stage, it is difficult to determine whether or not both 3D fissures (given by micro-CT and FIB/SEM) contribute to fluid transport.

Sample	Water imbibition	20mm diam. micro-CT	M.I.P.	5mm parallelepipedic micro-CT	2D SEM medium density zone	2D SEM high density zone	0.8mm rod micro-CT	FIB/SEM
Volume (or Area)	53.8 cm <sup>3</sup>	2.61 cm <sup>3</sup>	1.43 cm <sup>3</sup>	43.7mm <sup>3</sup>	6 mm <sup>2</sup>	6 mm <sup>2</sup>	0.216 microns <sub>3</sub>	26157 nm <sup>3</sup>
d <sub>peak</sub> (microns)	-	52.4	0.35 ; (60.3)	17.5	6	4	4	(0.06) ; 0.1
porosity (%)	2.8-3.2	1.016 +/- 0.36	4.89	1.88 +/-0.17	5.3 +/- 2.2	6.6 +/- 1.6	1.34 +/- 0.15	1.27 +/- 0.02

Table 1: Main characteristics of the pore structure of the same T-2390-82 sandstone sample.

## PERMEABILITY PREDICTION

Macroscopic permeability K is calculated in two steps. On the small scale, the fracture transmissivity is calculated by solving the Stokes equation on several portions of the measured connected fissures by micro-CT and FIB/SEM. A single phase Lattice Boltzmann code is used; according to the standard terminology, it is a D3Q19 code with two relaxation times; the classical bounce-back condition is used at the solid interface. Each sample is completed by its mirror image in order to avoid overall boundary effects. More details can be found in [10].

On the large scale, the density of fissures is estimated by three different means based on the number of intersections with scanlines, on the surface density of fissures and on the intersections between fissures per unit surface. These three means show that the network is relatively isotropic. They provide very close estimations of the density. Then, a general formula derived from systematic numerical computations [2] is used to derive the macroscopic dimensionless permeability which is proportional to the fracture transmissivity  $K = \sigma \alpha \Delta \rho'^2 / [R(1 + \beta \Delta \rho')]$  where  $\alpha = 0.037$ ,  $\beta = 0.155$ ,  $\Delta \rho' = \rho' - 2.3$ . R is a

measure of the lateral fracture extension.  $\rho'$  is the average number of intersections per fracture. A closely related application is given in [11].

The combination of the two previous results yields the dimensional macroscopic permeability. For the combination of 2D SEM and FIB/SEM, permeability predictions  $K$  range between  $3 \cdot 10^{-21}$  -  $6.2 \cdot 10^{-20} \text{ m}^2$  (3 to 62 nanoDarcy). This is three to four orders of magnitude smaller than actual gas permeability measurements. For the combination of 2D SEM and micro-CT, permeability is predicted at values ranging between  $6 \cdot 10^{-18}$  -  $7.4 \cdot 10^{-16} \text{ m}^2$  (6 to 740 microDarcy). This is in better agreement with experimental gas permeability on centimetric samples.

## CONCLUSION

For tight sandstone T-2390-82, the relevant pore structure for fluid transport is well described on two separate scales: (1) the fissure network is imaged and characterized by 2D SEM, (2) the individual fissure between quartz grains is characterized at a 350 nm size by M.I.P., which is the same order of magnitude as the 100nm opening given by FIB/SEM. This fissure scale contributes by three-four orders of magnitude less to transport than the micrometric fissure aperture obtained by micro-CT (of 4 microns wide). The latter provides macroscopic permeability prediction consistent with gas permeability identification on centimetric samples. This original approach needs to be validated on other tight sandstones to prove its generality.

## ACKNOWLEDGEMENTS

Financial support by GDFSUEZ E&P International SA is gratefully acknowledged. The SEM national facility available at the Centre Commun de Microscopie de Lille (France) is supported by the Conseil Regional du Nord-Pas de Calais, and by the European Regional Development Fund (ERDF).

## REFERENCES

1. Z. Duan, C. A. Davy, F. Agostini, L. Jeannin, D. Troadec, F. Skoczylas, *International Journal of Rock Mechanics and Mining Science*, Vol.65, pp.75-85, 2014.
2. P.M. Adler, J.-F. Thovert, V.V. Mourzenko: Fractured porous media, *Oxford University Press*, 2012.
3. X. T. Chen, Th. Rougelot, C.A. Davy, W. Chen, F. Agostini, F. Skoczylas and X. Bourbon, *Cement and Concrete Research*, Vol.39 (12), pp. 1139-1148, 2009.
4. W. Chen, J. Liu, F. Brue, F. Skoczylas, C. A. Davy, X. Bourbon, J. Talandier, *Cement and Concrete Research*, Vol.42, pp. 1001-1013, 2012.
5. Shafer J. and Neasham J. *Mercury Porosimetry International Symposium of the Society of Core Analysts*, 2000, SCA 2021.
6. Dewhurst D. N., Jones R. M. and Raven M. D. *Petroleum Geoscience*, 2002;8:371–383.
7. Holzer, L., Indutnyi, F., Gasser, P., Munch, B., and Wegmann, M. *Journal of Microscopy*, 216(1):84-95 (2004).

8. Y. Song, C. A. Davy, D. Troadec, A.-M. Blanchenet, F. Skoczylas, J. Talandier, J.-C. Robinet, *Marine and Petroleum Engineering*, 65 (2015) 63-82.
9. Munch, B. and Holzer, L. (2008). *Journal of the American Ceramic Society*, 91(12):4059–4067.
10. A. Pazdaniakou, P.M. Adler, Dynamic permeability of porous media by the lattice Boltzmann method, *Advances in Water Resources*, 62, 292, 2013.
11. I. Malinouskaya, J.-F. Thovert, V.V. Mourzenko, P.M. Adler, R. Shekhar, S. Agar, E. Rosero, M. Tsenn, Fracture analysis in the Amellago outcrop and permeability predictions, *Petroleum Geoscience*, 20, 93, 2014.